Multistep π Dimerization of Tetrakis(n-decyl)heptathienoacene Radical Cations: A Combined Experimental and Theoretical Study

ARTICLE *in* CHEMISTRY - A EUROPEAN JOURNAL · JULY 2014

Impact Factor: 5.73 · DOI: 10.1002/chem.201402182

10 AUTHORS, INCLUDING:

Marçal Capdevila-Cortada
ICIQ Institute of Chemical Research of Catal…
17 PUBLICATIONS **64** CITATIONS
SEE PROFILE

Russell Balster
Durham University
2 PUBLICATIONS **6** CITATIONS
SEE PROFILE

Juan J. Novoa
University of Barcelona
276 PUBLICATIONS **5,500** CITATIONS
SEE PROFILE

Juan Teodomiro López Navarrete
University of Malaga
335 PUBLICATIONS **5,249** CITATIONS
SEE PROFILE

ChemPubSoc Europe

DOI: 10.1002/chem.201402182

CHEMISTRY
A European Journal
Full Paper

Dimerization

Multistep π Dimerization of Tetrakis(*n*-decyl)heptathienoacene Radical Cations: A Combined Experimental and Theoretical Study

Cristina Capel Ferrón,[a] Marçal Capdevila-Cortada,[c] Russell Balster,[b] František Hartl,*[b] Weijun Niu,[d] Mingqian He,[d] Juan J. Novoa,[c] Juan T. López Navarrete,*[a] Víctor Hernández,*[a] and M. Carmen Ruiz Delgado*[a]

Abstract: Radical cations of a heptathienoacene α,β-substituted with four *n*-decyl side groups ($D4T7^{\bullet+}$) form exceptionally stable π-dimer dications already at ambient temperature (*Chem. Comm*. **2011**, *47*, 12622). This extraordinary π-dimerization process is investigated here with a focus on the ultimate $[D4T7^{\bullet+}]_2$ π-dimer dication and yet-unreported transitory species formed during and after the oxidation. To this end, we use a joint experimental and theoretical approach that combines cyclic voltammetry, in situ spectrochemistry and spectroelectrochemistry, EPR spectroscopy, and DFT calculations. The impact of temperature, thienoacene concentration, and the nature and concentration of counteranions on the π-dimerization process is also investigated in detail. Two different transitory species were detected in the course of the one-electron oxidation: 1) a different transient conformation of the ultimate $[D4T7^{\bullet+}]_2$ π-dimer dications, the stability of which is strongly affected by the applied experimental conditions, and 2) intermediate $[D4T7]_2^{\bullet+}$ π-dimer radical cations formed prior to the fully oxidized $[D4T7]_2^{\bullet+}$ π-dimer dications. Thus, this comprehensive work demonstrates the formation of peculiar supramolecular species of heptathienoacene radical cations, the stability, nature, and structure of which have been successfully analyzed. We therefore believe that this study leads to a deeper fundamental understanding of the mechanism of dimer formation between conjugated aromatic systems.

Introduction

In recent years, there has been a growing interest in the study of the π dimerization of conjugated radical cations[1–17] with a dual purpose: 1) elucidation of the nature of the charge-transport phenomena in p-doped semiconducting polymers, and 2) development of supramolecular bonding ideas for applications in material science, such as actuators.[18–23] In particular, π dimers of oligothiophene radical cations were proposed two decades ago to play a key role in electronic conduction of p-doped polythiophenes.[24] Investigations into the mechanism of the interaction between oligothiophene radical cations[1–8,25–30] deepen the understanding of the chemistry of this particularly attractive building block for organic electronics. For instance, it has been found that the tendency for intermolecular π dimerization can be attenuated and, in some cases, shut down when bulky groups are inserted in the β positions at thiophene rings;[31–34] note the evidence from X-ray crystallography that the closest intermolecular contact in the π dimer of nonhindered systems takes place at the central rings.[25,26,29] As a result of the attachment of bulky side groups, unfavorable steric interactions may occur, thereby preventing π oligomers from close intermolecular contacts leading to a sizeable π-orbital overlap upon oxidation, an arrangement that is nevertheless highly desirable to achieve a good p-type charge-carrier mobility.[35] However, the steric hindrance of dimerization of cationic π-conjugated oligothiophenes provides valuable information on the intrinsic properties of positively charged π systems in a segregated state and can be considered an important technique for the fabrication of "insulated molecular wires" in molecular devices.

Although oligo-/polythiophenes are key ingredients in the development of π-extended optoelectronic materials, deviation from planarity may decrease conjugation through the torsion of single bonds or S-*syn* defects.[36] Such defects do not arise in fully fused conjugated oligomers, such as pentacene, which nevertheless lacks environmental stability. In this context, oli-

[a] Dr. C. C. Ferrón, Prof. Dr. J. T. López Navarrete, Prof. Dr. V. Hernández, Dr. M. C. Ruiz Delgado
Department of Physical Chemistry, University of Málaga
Campus de Teatinos s/n, Málaga 29071 (Spain)
Fax: (+34) 952132000
E-mail: teodomiro@uma.es
hernandez@uma.es
carmenrd@uma.es

[b] R. Balster, Prof. Dr. F. Hartl
Department of Chemistry, University of Reading
Whiteknights, Reading (United Kingdom)
E-mail: f.hartl@reading.ac.uk

[c] M. Capdevila-Cortada, Prof. Dr. J. J. Novoa
Department de Química Física and IQTCUB
Facultad de Química, Universitat de Barcelona
Av. Diagonal 647, 08028 Barcelona (Spain)

[d] Dr. W. Niu, Dr. M. He
Corning Incorporated, SP-FR-6
Corning, New York, 14830 (USA)

Supporting information for this article is available on the WWW under http://dx.doi.org/10.1002/chem.201402182.

gothienoacenes, the fused-ring analogue of α-linked oligothiophenes, emerge as a promising new class of conjugated materials.[37–39] Their rigid and planar molecular structures tend to form densely packed solid-state structures that result in high charge-carrier mobilities.[35,38] However, fused thiophenes lead to lower solubility compared to the α-linked analogues. To solve this problem, some synthetic strategies have been reported in the literature over the past few years that incorporate the solubilizing tris(isopropyl)silyl (TIPS) or *n*-decyl substituents in the α- and/or β-terminal positions at the oligothienyl backbones.[38,40] Despite the large number of studies available on the π dimerization of oligothiophene radical cations, only a few examples are devoted to the study of the supramolecular arrangement of oligothienoacene radical cations. For instance, some of us recently demonstrated the formation of π-dimer dications in oxidized tetrathienoacenes,[41] pentathienoacenes,[42] and heptathienoacenes.[43] When compared to α-linked oligothiophenes, the high propensity towards π dimerization of oligothienoacene radical cations can be attributed to the rigid and planar structure that can maximize the intermolecular orbital overlap upon oxidation. Specifically, radical cations of a heptathienoacene α,β-substituted with four *n*-decyl side groups (D4T7) are shown to exhibit an exceptional capability for π-dimer formation even at room temperature.[43] Note that π dimerization of planar conjugated radical cations in solution is rare and is usually encountered only at low temperatures.[44–46]

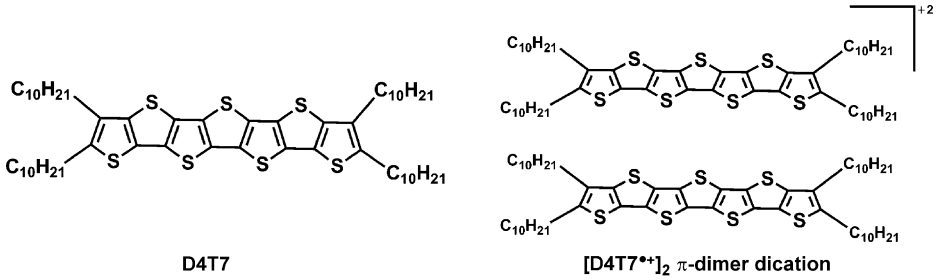

With the aim of improving the understanding of the mechanism of π-dimer formation in oligothienoacenes, we focus here on the π-dimerization process of radical cations of D4T7. The properties of the ultimate $[D4T7^{\bullet+}]_2$ π-dimer dication and yet-unreported transitory species formed during and after the oxidation are analyzed as a function of the temperature, the concentration of the heptathienoacene itself, and the concentration and nature of counterions; for instance, note that the stabilization of the radical cations is found to be strongly affected by the nucleophilic character of the counterions, which ultimately alters the dimer formation.[47] To this end, we used a combined experimental/theoretical approach that links cyclic voltammetry, in situ spectroelectrochemistry, and chemical doping methods (in particular UV/Vis-NIR and EPR monitoring) with density functional theory (DFT). Time-dependent (TD) DFT/ωB97XD calculations successfully provide a reliable assignment of the electronic absorption spectra of the ultimate π-dimer dication $[D4T7^{\bullet+}]_2$ and also the transitory species formed in the course of the D4T7 oxidation. In turn, this approach greatly aids the identification of their nature and structure.

Results and Discussion

Experimental evidence of transitory oxidized species

Different conformations of $[D4T7^{\bullet+}]_2$ π-dimer dications

Oxidations performed at low concentration of D4T7: The influence of different oxidants, an excess amount of counterions and their nature, and temperature variation

At the early stages of the UV/Vis-NIR spectral monitoring of the stepwise oxidation of approximately 10^{-5} M D4T7 ($E_{1/2} = +0.34$ V versus ferrocene/ferrocenium (Fc/Fc^+)) with one equivalent of the thianthrenium radical cation $TA^{\bullet+}$ added as the PF^{6-} salt ($TAPF_6$; $E_{1/2} = +0.82$ V versus Fc/Fc^+), the spectra show the appearance of two characteristic subgap absorptions at 582 and 1116 nm due to isolated radical cations $D4T7^{\bullet+}$ (Figure 1a). During the further addition of the solution of $TAPF_6$, a third broad and structureless subgap absorption appears at approximately 700 nm (Figure 1b), which is indicative of the formation of the ultimate π-dimer dication $[D4T7^{\bullet+}]_2$.[43] A similar spectral evolution towards π-dimer dication formation is encountered when using the $TASbCl_6$ oxidant (Figure 1c, d).

The impact of the counterions on the formation of the $[D4T7^{\bullet+}]_2$ π-dimer dication has been analyzed by inspecting the spectral changes recorded in the course of the one-electron oxi-

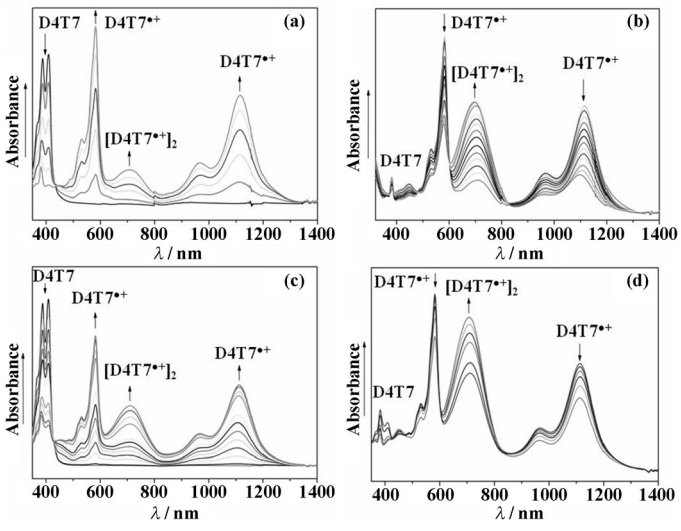

Figure 1. UV/Vis-NIR spectral changes recorded 1) in the course of the $1e^-$ oxidation of approximately 10^{-5} M D4T7 with 1 equiv a) $TAPF_6$ or c) $TASbCl_6$ in dichloromethane at room temperature, leading at the early stages to the dominant formation of isolated $D4T7^{\bullet+}$ together with a small fraction of $[D4T7^{\bullet+}]_2$; and 2) during the subsequent conversion of the radical cations into the π-dimer dications stabilized with b) PF_6^- and d) $SbCl_6^-$.

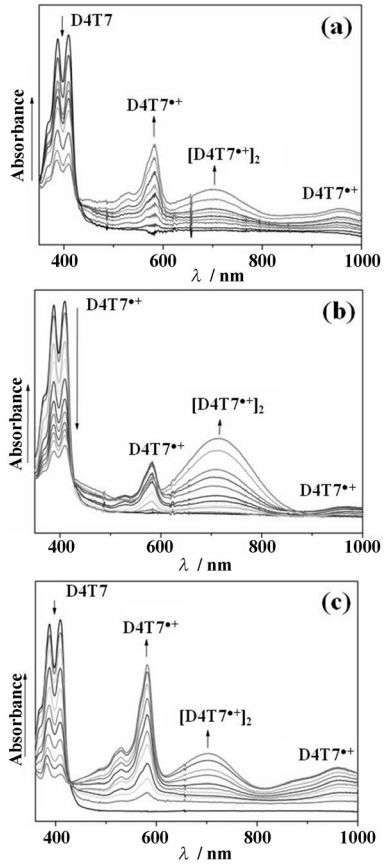

Figure 2. UV/Vis-NIR spectral changes recorded in the course of the stepwise $1e^-$ oxidation of approximately 10^{-5} M D4T7 with 1 equiv $TAPF_6$ in dichloromethane at room temperature in the presence of a) 5×10^{-2} M Bu_4NPF_6, b) 10^{-1} M Bu_4NPF_6, and c) 10^{-1} M $Bu_4N[B(C_6F_5)_{4]}$.

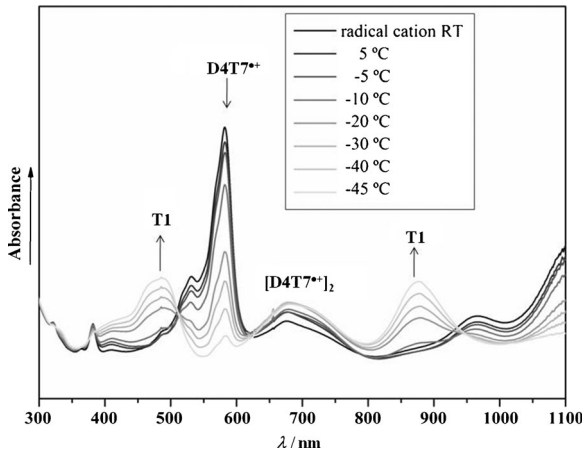

Figure 3. UV/Vis-NIR spectral changes recorded after the $1e^-$ oxidation of approximately 10^{-5} M D4T7 with $TAPF_6$ (1 equiv) in dichloromethane at room temperature, followed by rapid cooling of the solution that contained reactive $D4T7^{\bullet+}$. The absorption bands denoted as T1 belong to a transient π-dimer dication slowly converting to the ultimate $[D4T7^{\bullet+}]_2$ conformation.

dation of D4T7 with $TAPF_6$ in the presence of the supporting electrolytes tetrabutylammonium hexafluorophosphate, Bu_4NPF_6, or tetrakis(pentafluorophenyl)borate, $Bu_4N[B(C_6F_5)_4]$. In the presence of the counterions, as seen in Figure 2a–c, the broad absorption owing to the π-dimer dication increases rapidly in intensity relative to the Vis-NIR subgaps of the isolated radical cations. Although a similar upsurge of the $[D4T7^{\bullet+}]_2$ band is found at low PF_6^- concentrations (Figure 2a) and high $B(C_6F_5)_4^-$ concentrations (Figure 2c), this effect is more pronounced in the presence of a high excess amount of PF_6^- counterions (Figure 2b). Note that $B(C_6F_5)_4^-$ anions are considered as weakly coordinating (nucleophiles) and weakly ion-pairing;[48] thus, they tend to stabilize the radical cations and do not favor dimer dication formation owing to steric hindrance caused by their bulky structure.[49,50] Nonetheless, the formation of π-dimer dications is favored in the presence of both counteranions, the impact being more pronounced at high concentrations of PF_6^-. Identical behavior (i.e., the formation of the π-dimer dications from the very beginning of the monitoring sequence) has been observed during the in situ UV/Vis-NIR spectroelectrochemical oxidation of a low concentration (ca. 10^{-5} M) of D4T7 in the presence of a high excess amount of Bu_4NPF_6 as supporting electrolyte (see Figure S1 in the Supporting Information). Similar pairing enhancement effects caused by counterions were previously reported.[51,52]

Figure 3 shows the UV/Vis-NIR spectra recorded upon in situ chemical doping of D4T7 with $TAPF_6$ at various temperatures. As also found in the literature for nonfused oligothiophenes,[3,53] the tendency toward π dimerization of $D4T7^{\bullet+}$ increases with decreasing temperature. Upon cooling, the intensity of the two subgaps related to the radical cations decreased, and three new absorption bands appeared at 490, 681, and 876 nm; note that the band at 681 nm that belongs to the ultimate π-dimer dication is the only one observed at room temperature (compare with Figure 1a). These experiments have revealed the presence of a transient oxidized species T1 that absorbs at 490 and 876 nm and is stabilized at sufficiently low temperature. It could be assigned to a different conformation of the $[D4T7^{\bullet+}]_2$ π-dimer dication on the basis of evidence from concentration-dependent chemical and electrochemical oxidation experiments and TD-DFT calculations described in the following sections.

Chemical oxidation of D4T7 in dichloromethane with $TAPF_6$ under the experimental conditions that correspond to Figure 1a and b was also monitored with EPR spectroscopy. Only the signal of $D4T7^{\bullet+}$ was observed at $g=2.0026$ as a 1:4:6:4:1 quintuplet with $a_H=0.33$ mT (Figure 4). This hyperfine splitting pattern corresponds to the interaction of the unpaired electron with the proton nuclei of the two $-CH_2-$ groups attached to the terminal C_α atoms that bear significant spin density, unlike the C_β carbon atoms (Figure 5). The EPR signal of $D4T7^{\bullet+}$ slowly diminished in the course of its conversion to the $[D4T7^{\bullet+}]_2$ π-dimer dication. No other signal was detected in the course of the dimerization in this low-concentration region, not even upon cooling (compare with Figure 3), which proves that transient T1, much like the ultimate dimeric product $[D4T7^{\bullet+}]_2$, is a diamagnetic species.

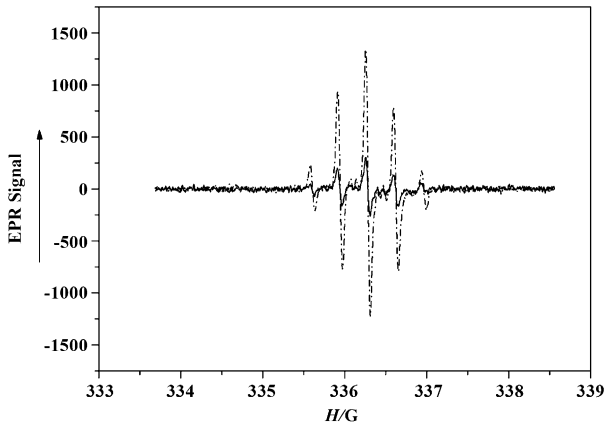

Figure 4. EPR spectra of $D4T7^{\bullet+}$ ($g = 2.0026$) recorded directly after the chemical oxidation of approximately 10^{-5} M D4T7 with $TAPF_6$ in dichloromethane (dashed line) and with a time delay of approximately 10 min (solid line). Experimental conditions: $T = 293$ K, microwave power of 4.0 mW, modulation frequency of 9.42 GHz.

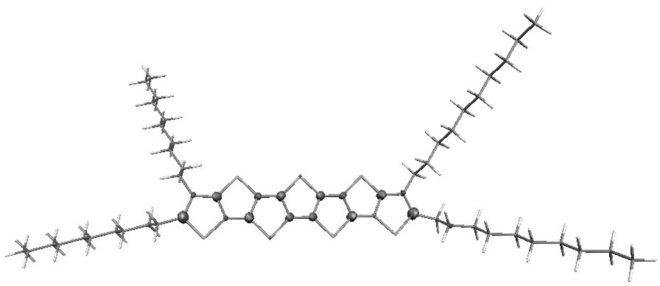

Figure 5. Spin-density distribution at the 0.01 a.u. isosurface of $D4T7^{\bullet+}$ calculated at the M06L/6-31G* level. Note the negligible spin density at the terminal C_β atoms.

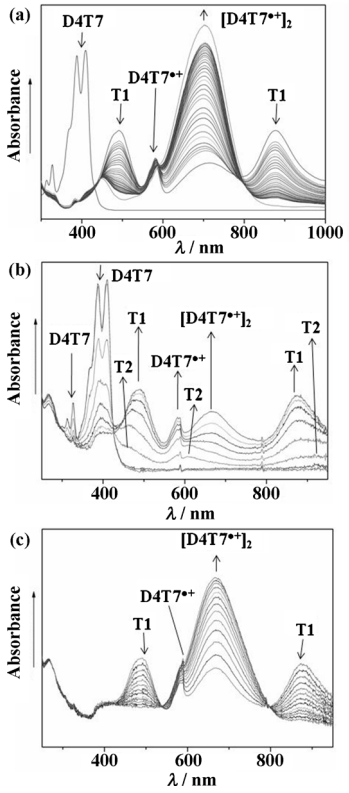

Figure 6. Rapid UV/Vis-NIR spectral changes recorded on the timescale of seconds directly after a) complete $1e^-$ oxidation of D4T7 (1.84×10^{-4} M) in dichloromethane with $TASbCl_6$, and b) rapid potential-step electrochemical oxidation of D4T7 (1.84×10^{-4} M) within an OTTLE cell ($T = 293$ K, CH_2Cl_2/3×10^{-1} M Bu_4NPF_6) in the early (left) and later (right) stages of the monitoring sequence.

Oxidations performed at high concentration of D4T7

To resolve the nature of the transient species T1 that absorbs at 490 and 876 nm (Figure 3) and was observed during the low-temperature doping experiments, we investigated the concentration-dependent spectral changes that accompanied the formation of $[D4T7^{\bullet+}]_2$. Figure 6a shows the UV/Vis-NIR spectra recorded in situ directly after the rapid chemical oxidation of 1.84×10^{-4} M D4T7 (considering $>10^{-4}$ M as the high concentration limit) with $TASbCl_6$ (1 equiv). The subgap absorption of $D4T7^{\bullet+}$ at 582 nm is diminished, and the UV/Vis spectrum reveals the three dominant absorption bands at 490, 681, and 876 nm, which are in compliance with Figure 3. The band at 681 nm owing to the ultimate π-dimer dication gains intensity over time at the expense of the absorption of the transient species. That is, the π-dimer dication is mainly formed from T1 while the remaining radical cation absorbing at 582 nm reacts more slowly and incompletely.

The spectral changes monitored upon the chemical oxidation were reproduced after rapid (potential-step) electrochemical oxidation of D4T7 in the high-concentration regime (around 2×10^{-4} M, comparable with the chemical doping; Figure 6a) in the presence of a high excess amount of PF_6^- in a thin-layer (ca. 0.2 mm) spectroelectrochemical cell (see Figure 6b). Similar to Figure 6a, both the ultimate π-dimer dication and the transient species T1 are observable from the very beginning of the monitoring sequence; later on, T1 transforms rapidly to the π-dimer dication. The conversion of T1 and $D4T7^{\bullet+}$ to the π-dimer dication is moderately faster in the presence of the excess amount of Bu_4NPF_6 electrolyte than that observed for the chemical doping with $TASbCl_6$.

However, the more bulky $Bu_4N[B(C_6F_5)_4]$ electrolyte causes somewhat slower conversion of the transient species T1 and the radical cation to the π-dimer dication (see Figure S2 in the Supporting Information); that is, the weakly coordinating $B(C_6F_5)_4^-$ anions stabilize $D4T7^{\bullet+}$ to a greater extent. However, the effect of the counterion nature and size seems to be less pronounced in the experiments performed at high concentrations of D4T7 ($\geq10^{-4}$ M) than encountered at low D4T7 concentrations (around 10^{-5} M), as previously shown in Figure 2b,c in which a direct conversion of the radical cations $D4T7^{\bullet+}$ to the $[D4T7^{\bullet+}]_2$ π-dimer dications is observed from the very beginning of the chemical oxidation (i.e., without the involvement of the intermediate and transient species).

Interestingly, back-reduction experiments led to the recovery of neutral parent D4T7 (see Figure S3 in the Supporting Information), with the bands of $D4T7^{\bullet+}$ and transient T1 disappearing first, followed by $[D4T7^{\bullet+}]_2$. That is, the most stable π-

dimer dication reduces less positively than the radical cation and T1. This conclusion from thin-layer spectroelectrochemistry has been confirmed by cyclic voltammograms recorded after chemical oxidation of D4T7 in CH_2Cl_2/TBAH with $TAPF_6$ at 253 K followed by slight temperature increase for solubility reasons. The irreversible cathodic wave of T1 was observed at $E_{p,c} = -0.19$ V versus Fc/Fc^+ at 273 K and the dominant one of $[D4T7^{\bullet+}]_2$ at $E_{p,c} = -0.63$ V (see Figure S4 in the Supporting Information). At 293 K only the back reduction of the ultimate oxidation product $[D4T7^{\bullet+}]_2$ was present at $E_{p,c} = -0.51$ V. The remarkably more negative reduction potentials of both T1 and $[D4T7^{\bullet+}]_2$ relative to $E_{1/2}$ ($D4T7^{0/\bullet+}$) attest to the large thermodynamic driving force of the π dimerization of $D4T7^{\bullet+}$, as also confirmed by DFT calculations (see above). The dimerization is promoted by the presence of dominant counterions, in particular, small and weakly coordinating PF_6^-, and also becomes facilitated by the high concentration of parent D4T7. The process also involves transient T1 (a different conformation of ultimate $[D4T7^{\bullet+}]_2$) that can be stabilized at low temperature. In the next section we will demonstrate that fully oxidized T1 is not the only transient species ascertained during the UV/Vis monitoring sequence.

Experimental evidence for partly oxidized $[D4T7]_2^{\bullet+}$ π-dimer radical cations

During the initial phase of the electrochemical oxidation of highly concentrated D4T7 (see Figure 6b), two new bands appeared at 470 and 620 nm before the upsurge of the three bands assigned to the π-dimer dications T1 and ultimate $[D4T7^{\bullet+}]_2$. These bands are attributed to additional species T2, the nature of which is revealed from combined results of 1) cyclic voltammetry, 2) the monitoring of the chemical and electrochemical oxidation experiments in which only a small portion of D4T7 is oxidized to the radical cation, and 3) a DFT study. As seen in Figure 7, when high-concentrated D4T7 starts to be oxidized either chemically (Figure 7a) or electrochemically (Figure 7b), the intermediate species T2 that absorbs at 470, 620, and 950 nm appears (together with some $D4T7^{\bullet+}$ in the absence of an excess amount of PF_6^- (Figure 7a) or when $B(C_6F_5)_4^-$ is used). The electronic absorption of T2 resembles a blend of parent D4T7 and $D4T7^{\bullet+}$. Note that chemically produced T2 (Figure 7a) converts slowly along with $D4T7^{\bullet+}$ directly to the ultimate π-dimer dication (upsurge of the band at 681 nm). However, electrochemically generated T2 is stable; only the further oxidation of D4T7 converted T2 to the ultimate π-dimer dications (Figure 6b). Given the fact that T2 can be generated at a high excess amount of neutral parent D4T7, it originates most likely from π coupling of a neutral parent D4T7 chain with its radical cation, thus leading to the formation of the $[D4T7]_2^{\bullet+}$ π-dimer radical cation in the initial phase of the oxidation. Upon further oxidation, π-dimer dications are directly formed from the $[D4T7]_2^{\bullet+}$ π-dimer radical cations (i.e., on the oxidation of the neutral heptathienoacene chain in the radical cation dimers bound to a previously formed minor amount of $D4T7^{\bullet+}$). The structure of $[D4T7]_2^{\bullet+}$ (=T2) has been resolved by DFT calculations, and the calculated TD-DFT electronic excitations appreciably reproduced its electronic absorption spectrum (Figure 7b).

A useful insight into the process of T2 formation was also obtained from cyclic voltammetry. Figure 8 shows the cyclic voltammogram of highly concentrated (2×10^{-4} M) D4T7 in $CH_2Cl_2/Bu_4N[B(C_6F_5)_4]$ together with the cobaltocenium (Cc^+)

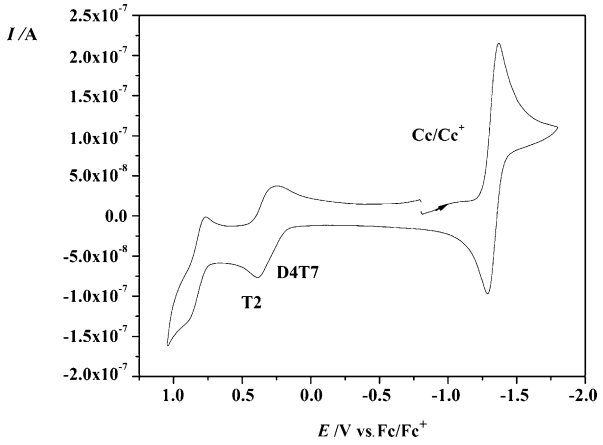

Figure 8. Cyclic voltammogram of 2×10^{-4} M D4T7 in $CH_2Cl_2/10^{-1}$ M $Bu_4N[B(C_6F_5)_4]$ recorded at $T = 293$ K and $v = 100$ mV s^{-1}. The working electrode was a carefully polished 0.125 mm^2 Pt disc. Cobaltocenium (Cc^+) hexafluorophosphate was used as an internal standard ($E_{1/2} = -1.33$ V versus Fc/Fc^+).

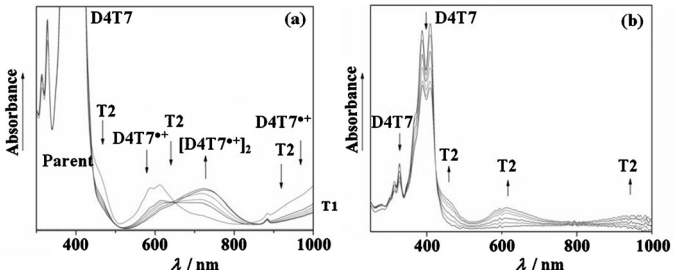

Figure 7. a) UV/Vis-NIR spectral changes recorded after the $1e^-$ oxidation of approximately 2×10^{-4} M D4T7 with a small amount of $TASbCl_6$ in dichloromethane in a 1 cm airtight cuvette. b) UV/Vis spectral monitoring of the electrochemical oxidation of 1.84×10^{-4} M D4T7 within an OTTLE cell ($T = 293$ K, $CH_2Cl_2/3\times10^{-1}$ M Bu_4NPF_6).

internal standard. Whereas the Nernstian Cc/Cc^+ redox couple represents a rapid and reversible electron transfer, the anodic response of D4T7 at approximately +0.3 V versus Fc/Fc^+ consists of two close-lying, poorly resolved anodic waves and cathodic counterwaves. On the basis of the spectroelectrochemical monitoring, the first anodic wave is assumed to correspond to the oxidation of free D4T7 to $D4T7^{\bullet+}$ (partly stabilized with $[B(C_6F_5)_4]^-$) and the slightly positively shifted wave to the oxidation of the second half of D4T7 in the concomitantly formed $[D4T7]_2^{\bullet+}$ π-dimer radical cation. On the timescale of cyclic voltammetry, the cathodic wave at −0.5 V due to back reduction of the resulting firmly π-bound dimer dication $[D4T7^{\bullet+}]_2$ is not detectable prior to the complete chemical oxi-

dation of D4T7 with thianthrenium radical cation salt, as described above.

Finally, the radical nature of the $[D4T7]_2^{\bullet+}$ π-dimer radical cation(T2) was also probed with EPR spectroscopy. Chemical oxidation of approximately 2×10^{-4} M D4T7 with $TAPF_6$ was carried out directly in the EPR spectroscopy tube in a special way by layering the oxidant solution over the D4T7 solution and letting blue radical cations $D4T7^{\bullet+}$ diffuse from the contact interphase into the EPR-active area that contained non-oxidized D4T7. The presence of the $[D4T7]_2^{\bullet+}$ π-dimer radical cation (compare with Figure 7a) was indicated by the presence of a foreign EPR signal (Figure 9) that overlapped that of dominant $D4T7^{\bullet+}$. The hyperfine structure of the EPR signal of $[D4T7]_2^{\bullet+}$ was not analyzed in detail.

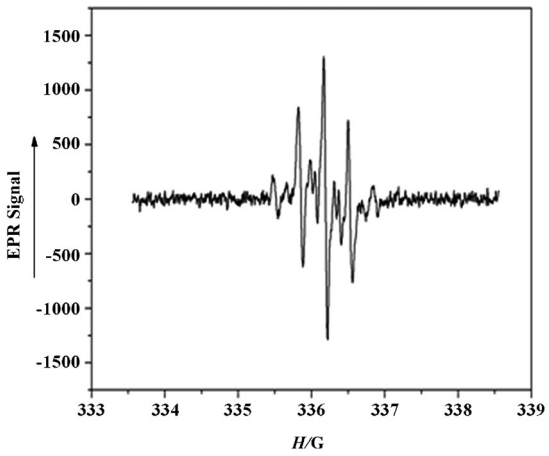

Figure 9. EPR spectrum of the solution layer in which radical cations $D4T7^{\bullet+}$ (compare with Figure 4) formed by chemical oxidation of approximately 2×10^{-4} D4T7 in dichloromethane with $TAPF_6$ interact with an excess amount of non-oxidized D4T7, forming the $[D4T7]_2^{\bullet+}$ radical cation dimer. Experimental conditions: $T=293$ K, microwave power of 4.0 mW, modulation frequency of 9.42 GHz.

DFT calculations of transitory oxidized species

To gain further insight into the structure and stability of the intermediate (T2) and transient (T1) oxidized species, density functional theory (DFT) calculations were conducted for the $[D4T7^{\bullet+}]_2$ π-dimer dications and $[D4T7]_2^{\bullet+}$ π-dimer radical cations. The solution environment is described by two models: 1) a polarizable continuum model (PCM) and 2) a discrete/continuum mixed model in which the $[D4T7^{\bullet+}]_2(CH_2Cl_2)_8$ or $[D4T7]_2^{\bullet+}(CH_2Cl_2)_8$ aggregates are combined with the PCM model. Three configurations (i.e., parallel, antiparallel, or X-shaped) for the spatial disposition of the two radical cations (or radical cation/neutral molecule in the case of the radical cation dimers) were considered. The impact of the orientations of the eight *n*-decyl side groups relative to the ring plane on the dimer stability was tested in our recent communication of $[D4T7^{\bullet+}]_2$ π-dimer dications in the parallel (*syn*), antiparallel (*anti*), and X-shaped configurations. Lateral and top views of their optimum structures are given in Figures S5–S7 of the Supporting Information. Both the continuous and mixed solvation models predict the *anti* and *syn* configurations to be stable against dissociation, with the accurate mixed description given more stable values by about 10–12 kcal mol^{-1}. However, both *anti* and *syn* configurations were found to be nearly isoenergetic, whereas the X-shaped configuration, in which the top radical cation, rotated by nearly 60° with respect to the main molecular axes of the bottom radical cation, is energetically unstable towards dissociation ($\Delta G_f^\circ = +4.1$ kcal mol^{-1}). This can be explained by the less efficient overlap of the SOMOs of the single chains in the X-shaped π-dimer dications relative to the cofacially superimposed *syn* and *anti* configurations. Additionally, the fact that the chains are not cofacially superimposed also reduces the dispersion attractive term of the interaction energy. The more accurate discrete/continuum mixed description cause the X-shaped aggregate to be stable towards dissociation by −9.5 kcal mol^{-1}, although it still remains 12 kcal mol^{-1} less stable than the *anti*/*syn* π-dimer dications.

With a view toward investigating the role played by the counterions, the free energies of formation of $[D4T7^{\bullet+}]_2(PF_6^-)_2(CH_2Cl_2)_4$ aggregates were obtained in a solution of dichloromethane (PCM; see Table 1). $[D4T7^{\bullet+}]_2(PF_6^-)_2(CH_2Cl_2)_4$ aggregates are about 3 kcal mol^{-1} more stable than $[D4T7^{\bullet+}]_2(CH_2Cl_2)_8$ aggregates, which confirms the stabilizing character of the PF_6^- counterions towards the π dimerization.

The stability of $[D4T7]_2^{\bullet+}$ π-dimer radical cations has also been explored and negative free energies of about −30 kcal mol^{-1} were obtained for both *anti* and *syn* conformations (see Table 1). The $[D4T7]_2^{\bullet+}$ radical cation dimers are therefore approximately 10 kcal mol^{-1} more stable than the $[D4T7^{\bullet+}]_2$ π-

Table 1. Free energy of formation values at 298 K of the $[D4T7^{\bullet+}]_2$ π-dimer dication in its *anti*, *syn*, and X-shaped configurations under different conditions: isolated, and in $(CH_2Cl_2)_8$ and $(PF_6^-)_2(CH_2Cl_2)_4$ aggregates. Free energy of formation (at 298 K) of the $[D4T7]_2^{\bullet+}$ π-dimer radical cation in its *anti* and *syn* orientations in $(CH_2Cl_2)_8$ aggregates are also given. All calculations are carried out in a continuous solvent environment (PCM, dichloromethane) at the M06L/6-31G(d) level.

Models[a]	*r* [Å][b]	ΔG_f° [kcal mol^{-1}]
	$[D4T7^{\bullet+}]_2$ π-dimer dication	
anti-$[D4T7^{\bullet+}]_2$	3.26	−10.4
syn-$[D4T7^{\bullet+}]_2$	3.31	−9.1
X-shaped $[D4T7^{\bullet+}]_2$	3.38	+4.1
anti-$[D4T7^{\bullet+}]_2(CH_2Cl_2)_8$	3.26	−21.0
syn-$[D4T7^{\bullet+}]_2(CH_2Cl_2)_8$	3.30	−22.5
X-shaped $[D4T7^{\bullet+}]_2(CH_2Cl_2)_8$	3.38	−9.5
anti-$[D4T7^{\bullet+}]_2(PF_6^-)_2(CH_2Cl_2)_4$	3.25	−24.1
syn-$[D4T7^{\bullet+}]_2(PF_6^-)_2(CH_2Cl_2)_4$	3.25	−25.5
X-shaped $[D4T7^{\bullet+}]_2(PF_6^-)_2(CH_2Cl_2)_4$	3.38	−11.7
	$[D4T7]_2^{\bullet+}$ π-dimer radical cation	
anti-$[D4T7]_2^{\bullet+}(CH_2Cl_2)_8$	3.30	−28.5
syn-$[D4T7]_2^{\bullet+}(CH_2Cl_2)_8$	3.35	−31.3
X-shaped $[D4T7]_2^{\bullet+}(CH_2Cl_2)_8$	3.40	−19.0

[a] An up-down-up-down (u-d-u-d) spatial disposition for the *n*-decyl groups was assumed for the *anti* and *syn* configurations, whereas a down-down-down-down (d-d-d-d) configuration was imposed for the three X-shaped models owing to steric hindrance. [b] Shortest C···C distance between adjacent D4T7 molecules in the dimer.

dimer dications, although the well-known self-interaction error for open-shell states on the pure DFT exchange functional might introduce a spurious overestimation of its energy.[54,55]

Time-dependent (TD) DFT calculations were then used to interpret the evolution of the electronic absorption spectra of the primary oxidation products D4T7$^{\bullet+}$ up to the [D4T7$^{\bullet+}$]$_2$ π-dimer dications through the formation of transient T1 (i.e., less stable conformations of [D4T7$^{\bullet+}$]$_2$ π-dimer dications: X-shaped configurations) and partly oxidized T2 intermediate species (i.e., [D4T7]$_2^{\bullet+}$ π-dimer radical cations). The ωB97XD long-range corrected functional was used in the TD-DFT calculations over the previous M06L-optimized structures. Note that TD-DFT/M06L provides a reliable description of the electronic absorption spectra of D4T7$^{\bullet+}$ but it has failed to closely reproduce the absorption spectra of the π-dimer dication, as shown in our previous work.[43]

As seen in Figure 10 (top), two intense electronic transitions were computed for D4T7$^{\bullet+}$ at 498 and 1013 nm, which closely match the experimental absorption bands measured at 582 and 1116 nm. For the isoenergetic *anti* and *syn* [D4T7$^{\bullet+}$]$_2$-$(CH_2Cl_2)_8$ aggregates, one intense band at 765 nm was predicted, which is associated with the (H−1→L) and (H−2→L) transitions; this band nicely reproduces the experimental broad band observed at approximately 700 nm for the ultimate π-dimer dication. For the less stable X-shaped [D4T7$^{\bullet+}$]$_2$-$(CH_2Cl_2)_8$ aggregate, two additional transitions at 497 and 976 nm were also obtained (Figure 10, bottom, and Table 2), which are in good accordance with the experimental bands observed at 490 and 876 nm that are associated with the formation of the transient oxidized species T1. Finally, for the *anti*-[D4T7]$_2^{\bullet+}$$(CH_2Cl_2)_8$ π-dimer radical cation, three bands are predicted at 394, 574, and 984 nm (Figure 10, bottom), in good agreement with the three experimental bands associated with the formation of the half-oxidized intermediate T2 (Table 2). Therefore, the TD-DFT calculations have reproduced reasonably well the experimental absorption spectra of the ultimate [D4T7$^{\bullet+}$]$_2$ π-dimer dication and the transient T1 and intermediate T2 species formed during the D4T7 oxidation.

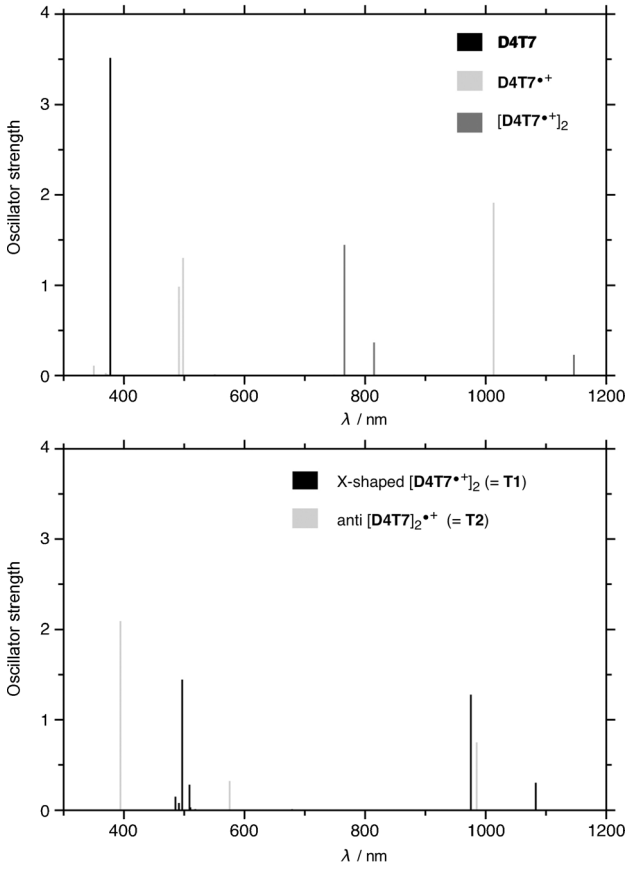

Figure 10. TD-DFT/ωB97XD-calculated vertical transition energies for top) neutral D4T7, the radical cation D4T7$^{\bullet+}$, and the *anti*-[D4T7$^{\bullet+}$]$_2$ π-dimer dication as the model for the ultimate dimer dication, and bottom) the X-shaped [D4T7$^{\bullet+}$]$_2$ π-dimer dication and the *anti* [D4T7]$_2^{\bullet+}$ π-dimer radical cation as the models for the transient T1 and half-oxidized intermediate T2 species, respectively.

Table 2. Observed and calculated absorption bands (λ [nm]) for neutral D4T7, the radical cation D4T7$^{\bullet+}$, the π-dimer dication [D4T7$^{\bullet+}$]$_2$, and the π-dimer radical cation [D4T7]$_2^{\bullet+}$.[a,b]

Compound	λ_{exptl} [nm]	λ_{calcd} [nm][a]
D4T7	388, 409	378
D4T7$^{\bullet+}$	582, 1116	498, 1013
[D4T7$^{\bullet+}$]$_2$	≈700[c]	765[d]
X-shaped [D4T7$^{\bullet+}$]$_2$ (=T1)	490, 876[e]	497, 976
anti-[D4T7]$_2^{\bullet+}$ (=T2)	470, 620, 950[f]	394, 574, 984

[a] Calculated at the TD-DFT//ωB97XD/6-31G(d) level. [b] A u-d-u-d spatial disposition for the *n*-decyl groups was assumed here for the *anti*-[D4T7$^{\bullet+}$]$_2$ π-dimer and *anti*-[D4T7]$_2^{\bullet+}$ radical cation dimer, and a d-d-d-d conformation was considered for the X-shaped [D4T7$^{\bullet+}$]$_2$ π dimer. [c] Ultimate π-dimer dication. [d] [D4T7$^{\bullet+}$]$_2$ π-dimer dication in its *anti* configuration. [e] Oxidized transient species T1. [f] Partly oxidized intermediate species T2.

Conclusion

The marked propensity towards π dimerization shown by the radical cations of an α,β-substituted heptathienoacene D4T7 in dichloromethane was investigated in detail by using a combined experimental and theoretical approach. The stability, nature, and spectroscopic characteristics of the ultimate π-dimer dications and transitory species formed in the course of the D4T7 oxidation were analyzed as a function of the temperature, D4T7 concentration, and the nature and concentration of counterions. Over the course of the one-electron oxidation of D4T7 up to the formation of the final π-dimer dication that absorbs at approximately 700 nm, two different transitory oxidized species were observed:

1) In addition to the band related to the ultimate π-dimer dication at approximately 700 nm, either in the low-temperature experiments for solutions of low concentration of D4T7 or in the room-temperature experiments for highly concentrated D4T7 solutions, two new bands appear at 490 and 876 nm that are associated with the less thermally stable (EPR-silent transient T1) conformation of the [D4T7$^{\bullet+}$]$_2$ π-dimer dication. The actual structure of these transient oxidized species is assumed to be very similar to the DFT-calculated X-shaped [D4T7$^{\bullet+}$]$_2$ configuration, which, upon increasing the tempera-

ture, converts into the more stable quasi-isoenergetic *anti* or *syn* aggregates, which are, by contrast, cofacially overlapped.

2) Intermediate $[D4T7]_2^{\bullet+}$ π-dimer radical cations (T2) are found to appear prior to the fully chemically oxidized ultimate $[D4T7^{\bullet+}]_2$ π-dimer dications under a specific concentration regime in which the D4T7 concentration is high and the conversion to $D4T7^{\bullet+}$ is low. Electrochemically, $[D4T7]_2^{\bullet+}$ can be obtained at higher concentrations. The electronic absorption of the intermediate species at 470, 620, and 950 nm is reproduced quite well by TD-DFT/ωB97XD calculations, which proved to be an indispensible tool for understanding its molecular structure.

In summary, this work provides fundamental knowledge of the π-dimerization process in oligothienoacene radical cations and it might help to explore new design strategies of π-dimer-based supramolecular architectures for organic electronics.

Experimental Section

Chemicals and reagents

Dichloromethane was freshly distilled from CaH_2 under a dry nitrogen atmosphere. The supporting electrolytes Bu_4NPF_6 (Aldrich) and $Bu_4N[B(C_6F_5)_4]$ were recrystallized twice from absolute ethanol and vacuum-dried at 80 °C overnight.

The *n*-decyl substituents in the α,β-terminal positions were prepared according to the literature.[38,40,56] The $SbCl_6^-$ and PF_6^- salts of the thianthrenium radical cation ($TASbCl_6$, $TAPF_6$) were prepared by the literature methods[57–59] and a modified literature procedure,[60] respectively; see the Supporting Information for more details.

Spectroelectrochemistry

Cyclic voltammograms were recorded at 298 K under an atmosphere of dry argon in an airtight three-electrode cell equipped with a 0.125 mm^2 Pt disk working electrode, a Pt coil counter electrode, and a silver wire pseudoreference electrode. Cobaltocenium hexafluorophosphate was used as an internal standard for the determination of electrode potentials and signalization of possible effects of adsorption or electrode passivation. The cell in a Faraday cage was connected to a computer-controlled EG&G PAR Model 283 potentiostat or a PGSTAT 302N potentiostat (Metrohm Autolab).

UV/Vis-NIR spectroelectrochemistry was carried at 293 K using an optically transparent thin-layer electrochemical cell[61] positioned in the sample compartment of a Scinco S3100 diode array spectrophotometer. The working electrode (Pt minigrid, 32 wires per cm) potential was controlled with a PA4 potentiostat (Laboratory devices, Polná, Czech Republic) or an EmStat 3 USB potentiostat (PalmSens BV, The Netherlands).

Spectroscopy

Conventional UV/Vis-NIR spectra were recorded in a 10 mm quartz cuvette (Hellma) placed in a Cary 5000 UV/Vis-NIR spectrophotometer at room temperature. Aliquots of a freshly prepared $TAPF_6$ or $TASbCl_6$ solution in CH_2Cl_2 were added dropwise to the sample solution in the cuvette. After each addition and stirring, a UV/Vis-NIR spectrum was recorded.

EPR spectra were recorded using a JEOL FR30 X-band EPR spectrometer. The samples of D4T7 in dichloromethane were oxidized with $TAPF_6$ directly in a narrow EPR tube under an atmosphere of dry argon. Thianthrenium radicals ($g = 2.0081$)[62] also served as the internal *g*-value standard.

Computational details

DFT calculations were carried out by means of the Gaussian 09 program[63] running on an SGI Origin 2000 supercomputer. The M06L functional[64] and the standard 6-31G(d) basis set were used.[65] The M06L functional was chosen on account of its ability to describe π–π interactions and estimate the energies of weak intermolecular interactions more efficiently than the B3LYP functional.[66,67] The chemical doping and electrochemical experiments were conducted in solutions in dichloromethane. Accordingly, we also evaluated the impact of the solvent interaction on the π dimerization of $D4T7^{\bullet+}$ radical cations by using two models: 1) a PCM that considers the solvent (dichloromethane) as a continuous medium with a dielectric constant and represents the solute by means of a cavity built with a number of interlaced spheres,[68,69] and 2) a discrete/continuous mixed model in which a $[D4T7^{\bullet+}]_2(CH_2Cl_2)_8$ aggregate is combined with the PCM.

To gain further insight into the role played by the counterions given high PF_6^- concentrations, the optimum structure and stability of $[D4T7^{\bullet+}]2(PF_6^-)_2(CH_2Cl_2)_4$ aggregates were determined in solution in dichloromethane (PCM).

Vertical electronic excitation energies were calculated by using the time-dependent DFT approach[70–71] with the ωB97XD[72] functional and the 6-31G(d) basis set in a PCM environment on the previously optimized M06L/6-31G(d) molecular geometries. The TD-DFT calculations of the $[D4T7]_2^{\bullet+}(CH_2Cl_2)_8$ and $[D4T7^{\bullet+}]_2(CH_2Cl_2)_8$ aggregates were lightened by removing the eight CH_2Cl_2 molecules, since the continuous solvent produces almost identical effects. Molecular orbital contours were plotted using Molekel 4.3.[73]

Acknowledgements

We thank Prof. William E. Geiger (University of Vermont) for providing us with the supporting electrolyte $Bu_4N[B(C_6F_5)_4]$. This work was financially supported by the MINECO of Spain (CTQ2012-33733 and MAT2011-25972), Generalitat de Catalunya (2009-SGR-1203). F.H. also thanks the University of Reading for financial support (project F3168024). M.C.R.D. thanks the MICINN for a "Ramón y Cajal" Research contract.

Keywords: density functional calculations · dimerization · EPR spectroscopy · oligothienoacenes · supramolecular chemistry

[1] J. J. Apperloo, R. A. J. Janssen, P. R. L. Malenfant, L. Groenendaal, J. M. J. Fréchet, *J. Am. Chem. Soc.* **2000**, *122*, 7042 – 7051.
[2] P. Bäuerle, U. Segelbacher, A. Maier, M. Mehring, *J. Am. Chem. Soc.* **1993**, *115*, 10217 – 10223.
[3] P. Bäuerle, U. Segelbacher, K.-U. Gaudl, D. Huttenlocher, M. Mehring, *Angew. Chem.* **1993**, *105*, 125 – 127; *Angew. Chem. Int. Ed. Engl.* **1993**, *32*, 76 – 78.
[4] J. Casado, K. Takimiya, T. Otsubo, F. J. Ramírez, J. J. Quirante, R. P. Ortiz, S. R. González, M. M. Oliva, J. T. López Navarrete, *J. Am. Chem. Soc.* **2008**, *130*, 14028 – 14029.
[5] T. Kaikawa, K. Takimiya, Y. Aso, T. Otsubo, *Org. Lett.* **2000**, *2*, 4197 – 4199.
[6] S. Klod, K. Haubner, E. Jahne, L. Dunsch, *Chem. Sci.* **2010**, *1*, 743 – 750.
[7] D. A. Scherlis, N. Marzari, *J. Phys. Chem. B* **2004**, *108*, 17791 – 17795.

[8] C. Videlot, J. Ackermann, P. Blanchard, J. M. Raimundo, P. Frère, M. Allain, R. de Bettignies, E. Levillain, J. Roncali, *Adv. Mater.* **2003**, *15*, 306 – 310.
[9] J. Iehl, M. Frasconi, H.-P. Jacquot de Rouville, N. Renaud, S. M. Dyar, N. L. Strutt, R. Carmieli, M. R. Wasielewski, M. A. Ratner, J.-F. Nierengarten, J. F. Stoddart, *Chem. Sci.* **2013**, *4*, 1462 – 1469.
[10] M. Souto, J. Guasch, V. Lloveras, P. Mayorga, J. T. López Navarrete, J. Casado, I. Ratera, C. Rovira, A. Painelli, J. Veciana, *J. Phys. Chem. Lett.* **2013**, *4*, 2721 – 2726.
[11] A. C. Fahrenbach, J. C. Barnes, D. A. Lanfranchi, H. Li, A. Coskun, J. J. Gassensmith, Z. Liu, D. Benítez, A. Trabolsi, W. A. Goddard, M. Elhabiri, J. F. Stoddart, *J. Am. Chem. Soc.* **2012**, *134*, 3061 – 3072.
[12] J. M. Lü, S. V. Rosokha, J. K. Kochi, *J. Am. Chem. Soc.* **2003**, *125*, 12161 – 12171.
[13] S. V. Rosokha, J. K. Kochi, *J. Am. Chem. Soc.* **2007**, *129*, 828 – 838.
[14] S. V. Rosokha, J. K. Kochi, *J. Am. Chem. Soc.* **2007**, *129*, 3683 – 3697.
[15] D. Small, V. Zaitsev, Y. S. Jung, S. V. Rosokha, M. Head-Gordon, J. K. Kochi, *J. Am. Chem. Soc.* **2004**, *126*, 13850 – 13858.
[16] C. Wang, S. M. Dyar, D. Cao, A. C. Fahrenbach, N. Horwitz, M. T. Colvin, R. Carmieli, C. L. Stern, S. K. Dey, M. R. Wasielewski, J. F. Stoddart, *J. Am. Chem. Soc.* **2012**, *134*, 19136 – 19145.
[17] V. Zaitsev, S. V. Rosokha, M. Head-Gordon, J. K. Kochi, *J. Org. Chem.* **2006**, *71*, 520 – 526.
[18] I. i. Garcia-Yoldi, J. S. Miller, J. J. Novoa, *J. Phys. Chem. A* **2009**, *113*, 484 – 492.
[19] J. Huang, S. Kingsbury, M. Kertesz, *Phys. Chem. Chem. Phys.* **2008**, *10*, 2625 – 2635.
[20] Y. Jung, M. Head-Gordon, *Phys. Chem. Chem. Phys.* **2004**, *6*, 2008 – 2011.
[21] E. R. Kay, D. A. Leigh, F. Zerbetto, *Angew. Chem.* **2007**, *119*, 72 – 196; *Angew. Chem. Int. Ed.* **2007**, *46*, 72 – 191.
[22] M. J. Marsella, *Acc. Chem. Res.* **2002**, *35*, 944 – 951.
[23] E. Smela, *Adv. Mater.* **2003**, *15*, 481 – 494.
[24] M. G. Hill, K. R. Mann, L. L. Miller, J. F. Penneau, *J. Am. Chem. Soc.* **1992**, *114*, 2728 – 2730.
[25] D. D. Graf, J. P. Campbell, L. L. Miller, K. R. Mann, *J. Am. Chem. Soc.* **1996**, *118*, 5480 – 5481.
[26] D. D. Graf, R. G. Duan, J. P. Campbell, L. L. Miller, K. R. Mann, *J. Am. Chem. Soc.* **1997**, *119*, 5888 – 5899.
[27] R. P. Kingsborough, T. M. Swager, *J. Am. Chem. Soc.* **1999**, *121*, 8825 – 8834.
[28] L. L. Miller, K. R. Mann, *Acc. Chem. Res.* **1996**, *29*, 417 – 423.
[29] D. Yamazaki, T. Nishinaga, N. Tanino, K. Komatsu, *J. Am. Chem. Soc.* **2006**, *128*, 14470 – 14471.
[30] G. Zotti, A. Berlin, G. Pagani, G. Schiavon, S. Zecchin, *Adv. Mater.* **1994**, *6*, 231 – 233.
[31] Y. Ie, M. Endou, S. K. Lee, R. Yamada, H. Tada, Y. Aso, *Angew. Chem.* **2011**, *123*, 12186 – 12190; *Angew. Chem. Int. Ed.* **2011**, *50*, 11980 – 11984.
[32] Y. Ie, A. Han, T. Otsubo, Y. Aso, *Chem. Commun.* **2009**, *0*, 3020 – 3022.
[33] K. Sugiyasu, Y. Honsho, R. M. Harrison, A. Sato, T. Yasuda, S. Seki, M. Takeuchi, *J. Am. Chem. Soc.* **2010**, *132*, 14754 – 14756.
[34] M. Tateno, M. Takase, M. Iyoda, K. Komatsu, T. Nishinaga, *Chem. Eur. J.* **2013**, *19*, 5457 – 5467.
[35] J. L. Brédas, J. P. Calbert, D. A. da Silva Filho, J. Cornil, *Proc. Natl. Acad. Sci. USA* **2002**, *99*, 5804 – 5809.
[36] N. DiCésare, M. Belletête, A. Donat-Bouillud, M. Leclerc, G. Durocher, *Macromolecules* **1998**, *31*, 6289 – 6296.
[37] E. G. Kim, V. Coropceanu, N. E. Gruhn, R. S. Sanchez-Carrera, R. Snoeberger, A. J. Matzger, J. L. Bredas, *J. Am. Chem. Soc.* **2007**, *129*, 13072 – 13081.
[38] X. Zhang, A. P. Côté, A. J. Matzger, *J. Am. Chem. Soc.* **2005**, *127*, 10502 – 10503.
[39] K. Takimiya, S. Shinamura, I. Osaka, E. Miyazaki, *Adv. Mater.* **2011**, *23*, 4347 – 4370.
[40] T. Okamoto, K. Kudoh, A. Wakamiya, S. Yamaguchi, *Org. Lett.* **2005**, *7*, 5301 – 5304.
[41] N. S. Rizalman, C. C. Ferron, W. Niu, A. L. Wallace, M. He, R. Balster, J. Lampkin, V. Hernandez, J. T. Lopez Navarrete, M. C. Ruiz Delgado, F. Hartl, *RSC Adv.* **2013**, *3*, 25644 – 25647.
[42] R. Malavé Osuna, M. C. Ruiz Delgado, V. Hernández, J. T. López Navarrete, B. Vercelli, G. Zotti, J. J. Novoa, Y. Suzuki, S. Yamaguchi, J. T. Henssler, A. J. Matzger, *Chem. Eur. J.* **2009**, *15*, 12346 – 12361.
[43] C. C. Ferrón, M. C. R. Delgado, V. Hernandez, J. T. L. Navarrete, B. Vercelli, G. Zotti, M. C. Cortada, J. J. Novoa, W. Niu, M. He, F. Hartl, *Chem. Commun.* **2011**, *47*, 12622 – 12624.
[44] L. Goor, P. Duijnen, C. Koper, L. Jenneskens, R. A. Havenith, F. Hartl, *J. Solid State Electrochem.* **2011**, *15*, 2107 – 2117.
[45] V. Khodorkovsky, L. Shapiro, P. Krief, A. Shames, G. Mabon, A. Gorgues, M. Giffard, *Chem. Commun.* **2001**, 2736 – 2737.
[46] A. Y. Ziganshina, Y. H. Ko, W. S. Jeon, K. Kim, *Chem. Commun.* **2004**, 806 – 807.
[47] F. Barrière, W. E. Geiger, *J. Am. Chem. Soc.* **2006**, *128*, 3980 – 3989.
[48] R. J. LeSuer, C. Buttolph, W. E. Geiger, *Anal. Chem.* **2004**, *76*, 6395 – 6401.
[49] I. Krossing, I. Raabe, *Angew. Chem.* **2004**, *116*, 2116 – 2142; *Angew. Chem. Int. Ed.* **2004**, *43*, 2066 – 2090.
[50] J. Yuasa, T. Suenobu, K. Ohkubo, S. Fukuzumi, *Chem. Commun.* **2003**, *0*, 1070 – 1071.
[51] J. N. Novoa, J. Ribas-Ariño, W. W. Shum, J. S. Miller, *Inorg. Chem.* **2007**, *46*, 103 – 107.
[52] S. V. Rosokha, J. Lu, T. Y. Rosokha, J. K. Kochi, *Phys. Chem. Chem. Phys.* **2009**, *11*, 324 – 332.
[53] P. Hapiot, P. Audebert, K. Monnier, J. M. Pernaut, P. Garcia, *Chem. Mater.* **1994**, *6*, 1549 – 1555.
[54] Y. K. Zhang, W. T. Yang, *J. Chem. Phys.* **1998**, *109*, 2604 – 2608.
[55] J. Gräfenstein, E. Kraka, D. Cremer, *J. Chem. Phys.* **2004**, *120*, 524 – 539.
[56] M. He, F. Zhang, *J. Org. Chem.* **2007**, *72*, 442 – 451.
[57] J. Beck, T. Bredow, R. T. Tjahjanto, *Z. Naturforsch. B* **2009**, *64*, 145 – 152.
[58] N. G. Connelly, W. E. Geiger, *Chem. Rev.* **1996**, *96*, 877 – 910.
[59] E. A. C. Lucken, *J. Chem. Soc.* **1962**, 4963 – 4965.
[60] H. J. Shine, B.-J. Zhao, J. N. Marx, T. Ould-Ely, K. H. Whitmire, *J. Org. Chem.* **2004**, *69*, 9255 – 9261.
[61] M. Krejčik, M. Daněk, F. Hartl, *J. Electroanal. Chem. Interfacial Electrochem.* **1991**, *317*, 179 – 187.
[62] J. Giordan, H. Bock, *Chem. Ber.* **1982**, *115*, 2548 – 2559.
[63] Gaussian 09, Revision B.01, M. J. Frisch, G. W. Trucks, H. B. Schlegel, G. E. Scuseria, M. A. Robb, J. R. Cheeseman, G. Scalmani, V. Barone, B. Mennucci, G. A. Petersson, H. Nakatsuji, M. Caricato, X. Li, H. P. Hratchian, A. F. Izmaylov, J. Bloino, G. Zheng, J. L. Sonnenberg, M. Hada, M. Ehara, K. Toyota, R. Fukuda, J. Hasegawa, M. Ishida, T. Nakajima, Y. Honda, O. Kitao, H. Nakai, T. Vreven, J. A. Montgomery, Jr., J. E. Peralta, F. Ogliaro, M. Bearpark, J. J. Heyd, E. Brothers, K. N. Kudin, V. N. Staroverov, R. Kobayashi, J. Normand, K. Raghavachari, A. Rendell, J. C. Burant, S. S. Iyengar, J. Tomasi, M. Cossi, N. Rega, J. M. Millam, M. Klene, J. E. Knox, J. B. Cross, V. Bakken, C. Adamo, J. Jaramillo, R. Gomperts, R. E. Stratmann, O. Yazyev, A. J. Austin, R. Cammi, C. Pomelli, J. W. Ochterski, R. L. Martin, K. Morokuma, V. G. Zakrzewski, G. A. Voth, P. Salvador, J. J. Dannenberg, S. Dapprich, A. D. Daniels, Ö. Farkas, J. B. Foresman, J. V. Ortiz, J. Cioslowski, D. J. Fox, Gaussian, Inc., Wallingford CT, **2009**.
[64] Y. Zhao, D. G. Truhlar, *J. Chem. Phys.* **2006**, *125*, 194101.
[65] M. M. Francl, W. J. Pietro, W. J. Hehre, J. S. Binkley, M. S. Gordon, D. J. Defrees, J. A. Pople, *J. Chem. Phys.* **1982**, *77*, 3654 – 3665.
[66] D. Benitez, E. Tkatchouk, I. Yoon, J. F. Stoddart, W. A. Goddard, *J. Am. Chem. Soc.* **2008**, *130*, 14928 – 14929.
[67] M. Capdevila-Cortada, J. J. Novoa, *Chem. Eur. J.* **2012**, *18*, 5335 – 5344.
[68] S. Miertuš, E. Scrocco, J. Tomasi, *Chem. Phys.* **1981**, *55*, 117 – 129.
[69] J. L. Pascual-ahuir, E. Silla, I. Tuñon, *J. Comput. Chem.* **1994**, *15*, 1127 – 1138.
[70] M. E. Casida in *Recent Advances in Density Functional Methods*, (Ed. D. P. Chong), World Scientific, Singapore, **1995**, p. 115.
[71] E. Runge, E. K. U. Gross, *Phys. Rev. Lett.* **1984**, *52*, 997 – 1000.
[72] J.-D. Chai, M. Head-Gordon, *Phys. Chem. Chem. Phys.* **2008**, *10*, 6615 – 6620.
[73] S. Portmann, H. P. Lüthi, *Chimia* **2000**, *54*, 766.

Received: February 14, 2014
Published online on ■■ ■■, 0000

FULL PAPER

Dimerization

C. C. Ferrón, M. Capdevila-Cortada, R. Balster, F. Hartl, W. Niu, M. He, J. J. Novoa, J. T. López Navarrete,* V. Hernández,* M. C. Ruiz Delgado**

■■ – ■■

Multistep π Dimerization of Tetrakis(*n*-decyl)heptathienoacene Radical Cations: A Combined Experimental and Theoretical Study

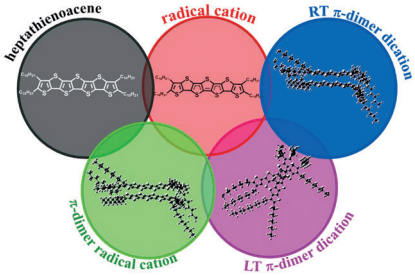

High propensity for π dimerization: Radical cations of an α,β-substituted heptathienoacene, D4T7, exhibit a high propensity for π dimerization, even at ambient temperature (see figure). Two different transitory oxidized species were detected: a less stable (low-T) conformation of the ultimate $[D4T7^{\bullet+}]_2$ π-dimer dications and intermediate $[D4T7]_2^{\bullet+}$ π-dimer radical cations. These observations are fully supported by DFT and time-dependent DFT calculations.